DESIGN OF A LOAD CELL WITH LARGE OVERLOAD CAPACITY

Farhad Aghili
Canadian Space Agency (CSA), Saint-Hubert, Quebec, Canada, J3Y 8Y9
E-mail: farhad.aghili@asc-csa.gc.ca

Received April 2010, Accepted October 2010
No. 10-CSME-24, E.I.C. Accession 3187

ABSTRACT

To increase the signal-to-noise (S/N) ratio and sensitivity of a load cell, it is desirable to design a structure that generates large strain close to maximum allowable strain of the sensor material for a given rating load force. However, accommodating the margin of safety with respect to overloading, compromises the sensitivity. This paper presents the design, analysis, and prototype testing of a load cell which can provide large overload protection capacity without compromising the sensitivity of the sensor. This is achieved by a special design of sensor structure that becomes virtually rigid after its flexures reach their maximum deflection, thereby the sensor can be protected against a large over load. The sensor dimensions, which maximizes the sensor's sensitivity, for given values of rating load and overload are obtained through mechanical strength analysis. A load cell prototype is fabricated and then tested to measure its linearity and overload characteristics. The experimental results show an accuracy of 0.2% of full scale and overload protection of the sensor flexures.

Keywords: load cell; force sensor; force transducer; overload protection.

CONCEPTION D'UNE CELLULE DE CHARGE AVEC UN GRAND CAPACITÉ DE SURCHARGE

RÉSUMÉ

Pour augmenter le rapport signal sur bruit et la sensibilité d'une cellule de charge, il est souhaitable de concevoir une structure qui génère des déformations avoisinant la limite permise du matériau pour une charge donnée. Toutefois, prendre en compte un facteur de sécurité par rapport à la surcharge peut compromettre la sensibilité. Cet article présente la conception, l'analyse et la validation expérimentale d'une cellule de charge pouvant fournir une protection contre la surcharge sans compromettre la sensibilité du capteur. Cela est atteint grâce à une conception particulière de la structure du capteur qui devient pratiquement rigide juste avant l'atteinte de l'état de déformation maximale, le capteur peut être ainsi protégé des surcharges. Les dimensions optimisant la sensibilité du capteur pour des valeurs de charge et de surcharge données sont obtenues d'une analyse de structure. Un prototype de cellule de charge est fabriqué puis testé afin de mesurer sa linéarité et ses caractéristiques de surcharge. Les résultats expérimentaux montrent une précision de 0.2% de la pleine échelle et une protection contre les surcharges en flexion du capteur.

Mots-clés : cellule de charge; capteur de force; protection contre les surcharges.

Nomenclature

D	ring diameter (m)
d	hub diameter (m)
E	Young's modulus (N/m^2)
F	force applied at the beam end point (N)
F_{axial}	axial force applied on the beams (N)
F_{cr}	buckling load of a beam with two of its ends clamped (N)
F_{overload}	maximum overload force capacity of the load cell (N)
F_{rating}	rating force of the load cell (N)
G_F	gauge factor of the strain gauges
h	beam's width-to-length ratio
I	second moment of inertia of the beams (m^4)
K	load cell stiffness (N/m)
L	beam length (m)
L_g	strain gauge length (m)
M	moment applied at the beam end point (Nm)
$M_b(x)$	moment applied to the beam at distance x (Nm)
R	strain gauge's resistance (Ω)
S	load cell sensitivity (1/N)
$S_{\max}$	optimal sensitivity (1/N)
t	beam thickness (m)
v	excitation voltage of Wheatstone bridge (volt)
Δv	output voltage of Wheatstone bridge (volt)
W	beam width (m)

Greek symbols

α	coefficient of thermal expansion
ΔT	temperature variation (°)
δ	beam deflection (m)
ε	strain
$\varepsilon_{\text{allow}}$	allowable strain of the load cell material
η	overload force to rating force ratio
σ_{allow}	allowable stress of the load cell material

1 INTRODUCTION

Load Cells, also known as force transducers, have a variety of applications in industry as well as R&D in science and technology. For example, they are used in vehicle and aerospace and automobile industry [1, 2, 3], industrial machinery, robotics and automation [4], civil and construction engineering [5], cable manufacturers, glass, iron & steel, power plants, metallurgy [6], mining, oil & gas, paper & pulp, gas or wind turbine [7], vibration detection, traffic monitoring [8], seismology [9], and military. Also, load cell are often used for weighting measurements in agriculture as well as food and animal product industry [10]. Many modern industrial machinery, turbines, as well as bridges, buildings, and dams are heavily instrumented by load cells either for structural health monitoring [5] or to check the exerted forces . Another interesting application of load cells is for the thrust measurement of rocket propellant systems [11, 12]. The nature of forces in some of these applications is rather uncertain so that the load cells may encounter unexpectedly large forces causing sensor breakdown. For example, it is reported that load cells for weighting objects show output failures approximately after one year of use [13].

In essence, load cells are fragile devices so as exceeding their force limits results in structural damage of the sensor. The overload capacity of many commercial load cells is not high enough for many industrial and laboratory applications. Therefore, in practice, an over sized sensor is chosen in order to increase the margin of safety with respect to overloading. However, the larger sensors are usually the less accurate one. The vast majority of commercial load cells (e.g. the produces of Omega Eng. Inc. [14] or S. Himmelstein and Company [15] or Interface Force

Measurement Ltd. [16]) are designed based on maximum strain/stress corresponding to 1.5 times of maximum load. This accommodates the load cell sensor with only 150% safe overload capacity. In order to boost the overload capacity, one may design a structure which generates less stress, and strain, in response to the load. But that compromises the sensitivity of the sensor. Another existing solution offered by Inter Technology is to use a shunt non-linear spring supporting the load cell [17]. The non-linear spring abruptly collapses in case of overloading that shunts the excess of rating load to built-in mechanical stops.

In general, force measurement is derived from strain measurement at location on an elastic sensor body. To increase the signal-to-noise (S/N) ratio and sensitivity of the sensor, it is desirable to design a structure that generates large strain close to maximum allowable strain of the sensor material for the maximum load force. However, a sensor designed based on such a specification doesn't bear any overload. Therefor, in order to accommodate the margin of safety with respect to overloading, the sensor must be designed for a load much higher than the rating load and that inevitably compromises the sensitivity of the sensor. The design solution based on the concept of non-linear spring is claimed to be able to provide overload capacity five time as much as the rating load [17]. This is high, but not sufficient in many practical cases especially where an impact force is involved. Moreover, such a protector mechanism is bulky and expensive and hence not suitable for miniature sensor.

This paper presents the design and analysis of a load cell which provides large overload protection capacity without compromising the sensitivity or affecting the characteristic of the sensor. The senor becomes virtually rigid after the sensor's flexures reach their maximum deflection, thereby the sensor can be protected against a large over load. Stress-stain analysis of the sensor was used to find the optimal dimensions of the sensor for a given rating load that maximizes the sensor sensitivity. A sensor prototype has been fabricated and subsequently has been undergone the linearity and overload tests. This paper is arranged as follows: Section 2 described the mechanical design of the load cell. Section 3 is devoted to mathematical modeling of the sensor used to calculate the optimal dimensions of the sensor with respect to a given earing load force. Finally, description of a load cell prototype and experimental validation of the sensor characteristics are presented in Section 4.

2 SENSOR DESIGN

Figure 1 illustrates the exploded view of the sensor design with a hub-sprocket shape. The transducing element is strain gauge, while the structure of the sensor is comprised of three parts: hub-sprocket, donut shim, and solid disk that are bolted together. The sprockets (or beams) connect the inner hub to the rigid ring. They also constitute the sensor flexures on which the strain gauges are cemented. Fig. 2 depicts schematically how the sensor functions (the beam deflection is exaggerated). The hub and the ring have identical thickness, hence their flat surfaces can site on a single plane. However, as shown in the Fig. 2A, the shim creates a gap between the hub and the flat surface of the rigid disk. That permits to deflect the flexure beams up to exactly the thickness of the shim. The shim thickness is chosen to be coincident with the maximum beam deflection corresponding to the rating load. Therefore, in case of overload, the hub flat surface reaches the disk; shunting the excess of the load to the disk, see Fig. 2B. Since normally there is no contact between the hub and disk, the mechanical stop does not affect the dynamics respond of the sensor whatsoever. The overload capacity of the sensor depends on the hub cross-section area, which can be arbitrarily chosen to be large enough. Also, the proposed sensor structure features high stiffness and excellent rejection of the extraneous loads,

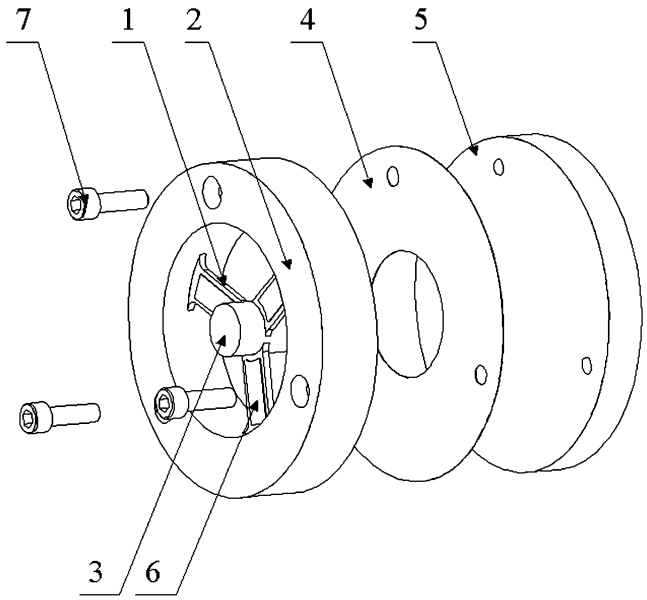

Fig. 1. The exploded view of the load cell: flexure beam (1); solid ring (2); hub (3); shim (4); solid disk (5); stain gauge (6); bolt (7).

i.e. non-axial components of the external load, assuring precision. The former is because the flexure beams are clamped at both ends (instead of the commonly used cantilever beam), while the latter is because of the symmetry of the sensor geometry. This in conjunction with additive properties of the Wheatstone bridge permits decoupling of output from extraneous force without any subsequent arithmetic.

3 MATHEMATICAL MODEL OF THE SENSOR

Figure 3 schematically shows one of the sensor's flexures. The flexures are primarily subjected to bending when external force is applied. Therefore, they are modeled as a beam whose left and right ends are clamped to the rigid ring and to the solid hub, respectively. Let F denote the external axial force applied to the load cell sensor which has three flexure beams. Due to the symmetric geometry of the sensor, the applied force is evenly distributed among the three beams. Hence each beam is subjected to shear force $\frac{1}{3}F$ and moment M at its end point. That is, the bending moment along the beam is $M_b(x)=\frac{1}{3}Fx-M$. The differential equation describing the deflection of a beam can be written by [18]

$$y''(x)=\frac{1}{EI}\left(\frac{1}{3}Fx-M\right), \tag{1}$$

where E is the Young's modulus, and I is the beams second moment of area. Let L denote the beam length; it is apparent from Fig. 2 that $L=\frac{D-d}{2}$, where D and d are the ring and the hub diameters, respectively. Since the beam's both ends are clamped, the boundary conditions are given by $y'(0)=0$ and $y'(L)=0$. Incorporating these boundary conditions on the integration of (1) yields

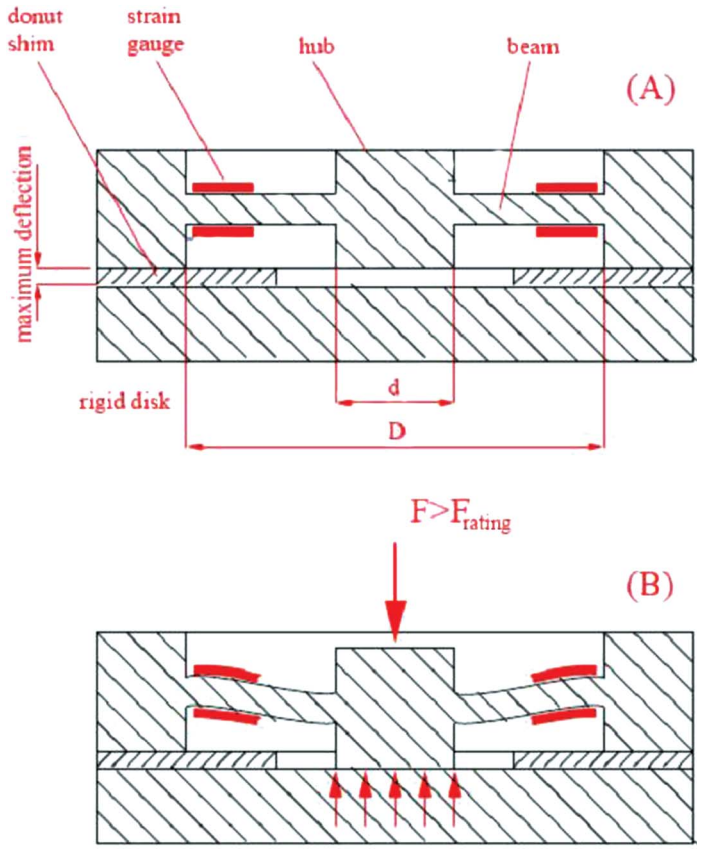

Fig. 2. The cross section view of the sensor: (A) no deflection, (B) maximum deflection.

$$M = \frac{1}{6}FL \tag{2}$$

Moreover, by incorporating the other boundary condition $y(L) = 0$ on the second integral of (1), one can found the beam's end-point deflection $\delta = y(0)$ to be

$$\delta = \frac{FL^3}{36EI} \tag{3}$$

Let us consider v and as G_F the excitation voltage of the strain gauges in Wheatstone bridge circuit, and the gauge factor of the strain gauges[1], respectively. Then, the output voltage of a half-bridge circuit, Δv, is given by

[1] The gauge factor is used to quantify strain gauges:

$$G_F = \frac{\partial R/R}{\partial L_g/L_g},$$

where R and L_g are the strain gauge's resistance and length. For typical foil strain gauge $G_F = 2.0$

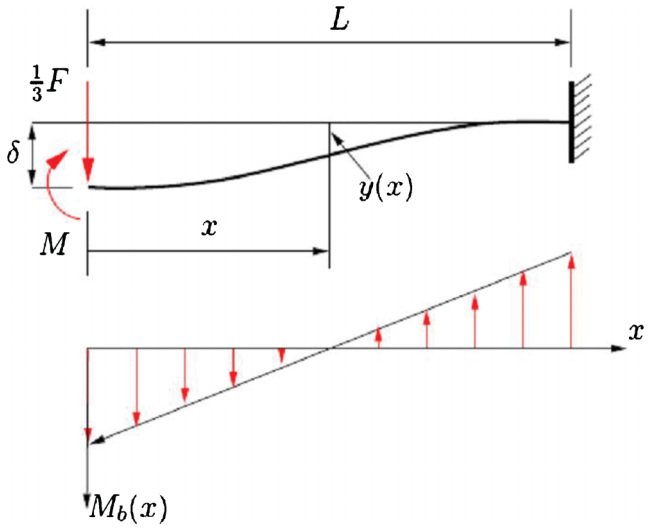

Fig. 3. One of the sensor's flexure.

$$\frac{\Delta v}{v} = G_F \bar{\varepsilon}, \tag{4}$$

where $\bar{\varepsilon}$ is the strain average under the strain gauge detecting area. The sensitivity of the load cell is defined as

$$S = \frac{\Delta v / v}{F} = \frac{G_F \bar{\varepsilon}}{F} \tag{5}$$

The strain induced along the beam as a function of distance is equal to

$$\varepsilon(x) = -\frac{M_b(x)t}{2EI} = \frac{Ft}{6EI}\left(\frac{1}{2}L - x\right), \tag{6}$$

where t is the thickness of the the beams. Since strain gauges average the strain field over their area, we need to integrate (6) over the gauge length of the strain gauges, L_g, to obtain the load cell sensitivity, i.e.,

$$\bar{\varepsilon} = \frac{1}{L_g}\int_0^{L_g} \varepsilon(x)dx = \frac{\kappa t L}{12EI}F, \tag{7}$$

where

$$\kappa = 1 - \frac{L_g}{L} \tag{8}$$

On the other hand, it is apparent form (6) that the maximum strain occurs at $x = 0$, i.e.,

$$\varepsilon_{\max} = \frac{tL}{12EI}F_{\text{rating}}, \tag{9}$$

where F_{rating} is the rating load force of the sensor. The maximum allowable strain for foil strain gauge is typically 3%, which is at least one order of magnitude higher that that of industrial metals, $\varepsilon_{\text{allow}}$, making the materials the limiting factor. Because a linear response is desired from the sensor, the chosen sensor material must have a linear strain-stress relationship. Steel is the best available industrial material that has good linearity properties within a large stress range. Moreover, due to the oscillatory nature of the force, steel can work with infinite fatigue life as the allowable stress (or equivalently strain) determined based on endurance limit corresponds to infinite lifetime. The maximum induced strain must be maintained lower than the allowable strain, i.e. $\max\varepsilon \leq \varepsilon_{\text{allow}}$. However, in order to gain maximum sensitivity

$$\varepsilon(0)|_{F=F_{\text{rating}}} = \varepsilon_{\text{allow}}. \tag{10}$$

Increasing the S/N ratio of the sensor output requires maximizing the sensor sensitivity. In view of (5), (7), (9) and (10), the maximum achievable sensitivity is given by

$$S_{\max} = \frac{\kappa G_F \varepsilon_{\text{allow}}}{F_{\text{rating}}} \tag{11}$$

In our design, the beam has rectangular cross section with width of W, hence

$$I = \frac{Wt^3}{12}. \tag{12}$$

Substituting (12) into (7) and then into (5) yields

$$S = \frac{\kappa G_F L}{EWt^2} \tag{13}$$

The goal is to design the load cell for maximum sensitivity. Therefore, by equating the right-hand sides of (11) and (13) we arrive at

$$S = S_{\max} \quad \Rightarrow \quad \frac{\varepsilon_{\text{allow}}}{F_{\text{rating}}} = \frac{L}{EWt^2}$$

Hence, the maximum sensitivity can be archived if the beam thickness satisfies the following identity

$$t = \sqrt{\frac{F_{\text{rating}}}{h\sigma_{\text{allow}}}}, \tag{14}$$

where $h = W/L$ is beam's width-to-length ratio and $\sigma_{\text{allow}} = E\varepsilon_{\text{allow}}$ is the corresponding maximum allowable stress. Finally, substituting (14) into (12) and then into (3) yields the sensor's full scale deflection

$$\delta_{\max} = \frac{L^2 \varepsilon_{\text{allow}}}{3} \sqrt{\frac{h\sigma_{\text{allow}}}{F_{\text{rating}}}} \tag{15}$$

It should be pointed out that the shim thickness, b, should be selected equal to the full-scale deflection. In order to achieve maximum sensor stiffness, it is desirable to have δ_{max} small as much as possible. However, from a practical point of view the minimum full-scale deflection is limited by the quality of machined surfaces and machining tolerances. Thus, for a given shim thickness $b=\delta_{max}$, the flexure length and thickness can be calculated from

$$L=\left(\frac{F_{rating}}{h\sigma_{allow}}\right)^{\frac{1}{4}}\sqrt{\frac{3b}{\varepsilon_{allow}}} \tag{16}$$

$$\frac{t}{L}=\frac{\varepsilon_{allow}}{3b}L \tag{17}$$

It is worth mentioning that the hub-sprocket design of the sensor is prone to thermal stresses that may result in beam bucking if the thickness is small. It can be shown that for this structure, the bucking can be avoided if $t/L>0.02$ (see the Appendix for details), that can be checked by making use of (17). The stiffness of the load cell can be readily calculated from

$$K=\frac{F_{rating}}{b} \tag{18}$$

It is interesting to note that combining (11) and (18) together reveals that the maximum sensitivity is inversely proportional to the stiffness regardless of the size of the load cell, i.e.,

$$S_{max}=\left(\frac{\kappa G_F \varepsilon_{allow}}{b}\right)\frac{1}{K}$$

As illustrated in the structure of sensor in Fig. 2, the flexures take all the load force exerted to the load cell up to $F\le F_{rating}$. However, in the case of overloading, i.e., $F_{overload}>F_{rating}$, the excess of load $F_{overload}-F_{rating}$ is shunted through the hub-disk contact. Therefore, the maximum overload force corresponding to the maximum bearing stress, σ_{allow}, can be calculated by

$$F_{overload}-F_{rating}=\frac{\pi}{4}\sigma_{allow}d^2$$

where d is the hub diameter. Thus, the overload capacity of the sensor can be calculated from

$$\eta := \frac{F_{overload}}{F_{rating}}=1+\frac{\pi\sigma_{allow}d^2}{4F_{rating}}, \tag{19}$$

and hence

$$d=1.13\sqrt{\frac{(\eta-1)F_{rating}}{\sigma_{allow}}}. \tag{20}$$

The intersection of the three flexures with width W at the center of the sensor virtually makes the vertices of an equilateral triangle. The radius of the circumcircle of such a triangle is equal to $\frac{\sqrt{3}}{3}W$. The circumcircle must be enclosed within the circular hub to have a geometry consistent with the baseline design in Fig. 2. Therefore, the geometry of a sensor with three flexures imposes the following constraint

$$W \le \frac{\sqrt{3}}{2}d \quad \Rightarrow \quad \frac{d}{L} \ge 1.15h \tag{21}$$

Substituting L and d respectively from (16) and (20) into the latter inequality of (21) yields

$$\eta > 1 + 3.1b\sqrt{\frac{Eh^3}{\varepsilon_{\text{allow}}F_{\text{rating}}}}, \tag{22}$$

which specifies the minimum overload ratio ensuring the geometry consistency (21).

Now, for a given sensor rating, F_{rating}, and overload ratio, η, a proper set of the dimension parameters $\mathscr{P}=\{h, L, t/L, d\}$ can be determined iteratively using equations (16), (17), and (20) subject to inequality constrain (22). The curves in Fig. 4 illustrate the load cell dimensions versus rating load corresponding to material properties $E=200$ GPa, $\varepsilon_{\text{allow}}=0.3\%$ and the strain gauge parameters $G_F=2.0$, $\kappa=0.75$ and shim thickness $b=0.3$ mm. The load cell dimensions and the corresponding characteristics for a wide range of rating loads are listed in Table 1.

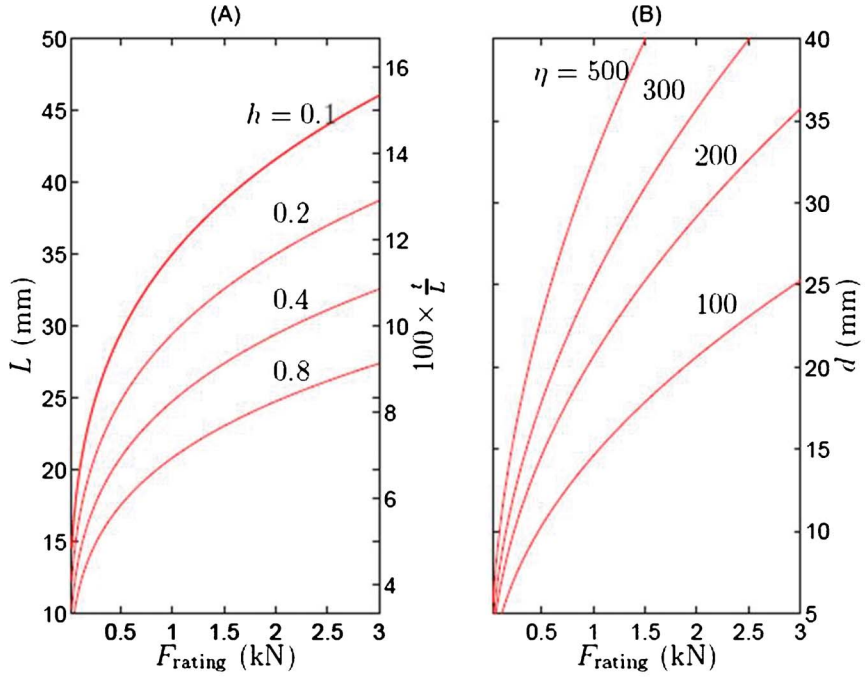

Fig. 4. The beam length (A) and hub diameter (B) versus different rating loads.

Table 1. Dimensions and characteristics of a series of load cells.

Load (N)	D^* (mm)	d (mm)	t (mm)	W (mm)	Overload ratio	S (mV/V/N)
30	33	10	0.4	3.3	800	0.15
300	57	17	1.3	5.9	200	1.5×10^{-2}
3000	109	38	4.1	10.5	100	1.5×10^{-3}
30000	170	61	10.0	27	25	1.5×10^{-4}
300000†	490	173	25	126	20	1.5×10^{-5}

* $D=2L+d$ is the load cell diameter.
† shim thickness $b=1.0$ mm, for other load cases $b=0.3$ mm.
$E=200$ GPa, $\sigma_{\text{allow}}=600$ MPa, $G_F=2.0$, $\kappa=0.75$.

4 SENSOR PROTOTYPE AND TESTING

Figures 5 and 6 illustrate a load cell prototype and its parts designed for rating load 30 N. The design parameters of the sensor and its dimensions are quoted in the first row of Table 1. The sensor body is a monolithic structure; that is, it is machined from a solid piece of metal. This decreases the hysteresis and increases the strength and repeatability of the sensor. The donut shim with thickness of $b=0.3$ mm creates the required gap between the sensor hub and the flat surface of the disk. A pair of foil stain gauges (SG-3/350-LY11 from Omega [14]) are cemented at the fixed-end location of each beams, while the strain gauges of the three beams are configured as series resistors by completing the bridge wiring inside the sensor; see Fig. 5. The strain gauges bridge is excited by a precisely regulated 8.0 VDC voltage.

The sensor prototype has been undergone linearity and overload tests. To characterize the linearity and sensitivity of the sensor, the sensor outputs in response to known weight loads are

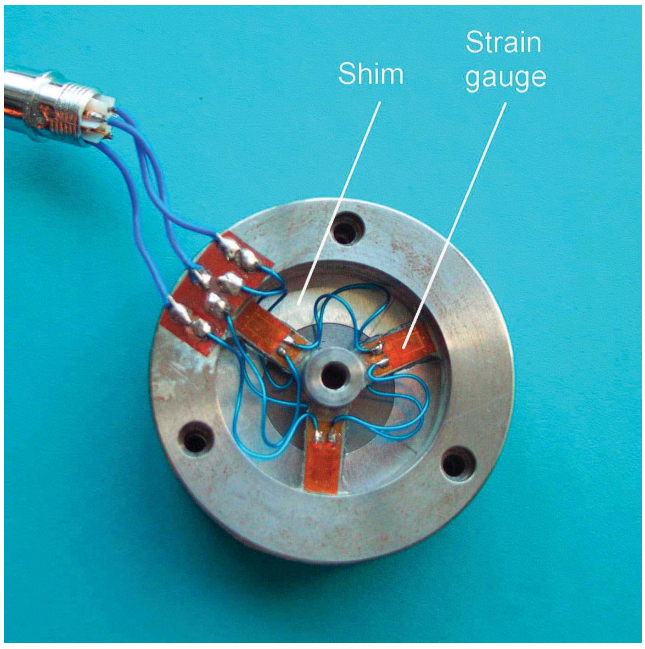

Fig. 5. The load cell prototype.

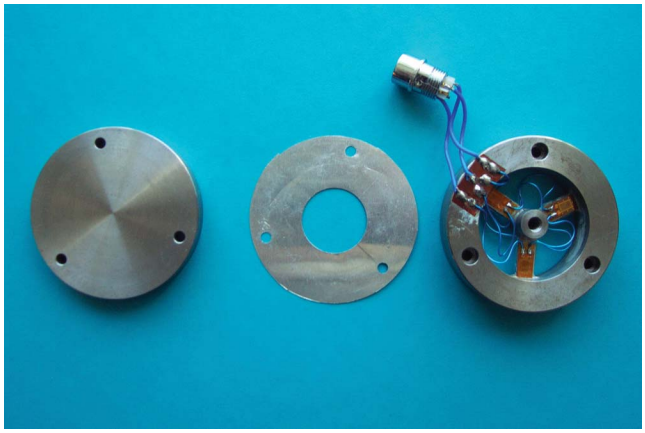

Fig. 6. The sensor components: body of sensor (A), shim (B), rigid disk (C).

measured. The load forces are applied to the load cell using a high-precision standard weight set. The load cell is connected to a laboratory Wheatstone bridge instrument equipped with an analog amplifier to boost the signal level of the bridge with factor of 100. The measured voltages corresponding to the masses of the weight set and the deviation from linearity are given in Table 2. The data shows that all collective deviation from linearity are about 0.2% full scale. The slope of a line passing through the data points indicates that the sensitivity of the sensor is 1.13 mV/N. Since the excitation voltage is 8 V, the theoretical sensitivity can be readily obtained from the first row of Table 1 to be 1.20 mV/N, which is in a close agreement with the measured sensitivity 1.13 mV/N. In the second part of the test, the load cell is overload by three weights above the sensor rating force. The load cell output voltages against underload forces and overload forces are depicted in Fig. 7. It is clear from that graph that the sensor output voltage saturates when the applied exceeds the rating load force 30 N. This observation support the fact that the excess load is shunted by sensor hub and hence the flexures must carry only the rating force portion of the overload force.

However, it is evident from Fig. 7 that there is slight slope in the response of the sensor after overloading. It should be notated that in the case of overloading, the excess of rating force is shunted by the hub, which is now under compression. Although the hub is very stiff compared to the flexure, the stiffness is not infinite and hence the compression cases minute deformation even when the hub flat surface reaches the disk.

Table 2. Sensor calibration data.

Weight mass (Kg)	$100 \times v_o$ (volt)	Deviation from linearity (FS) %
0.5	0.561	0.11
0.75	0.845	0.06
1.0	1.123	0.19
1.25	1.406	0.18
1.50	1.688	0.18
1.75	1.971	0.17
2.00	2.255	0.09
2.50	2.830	0.21
3.00	3.396	0.24

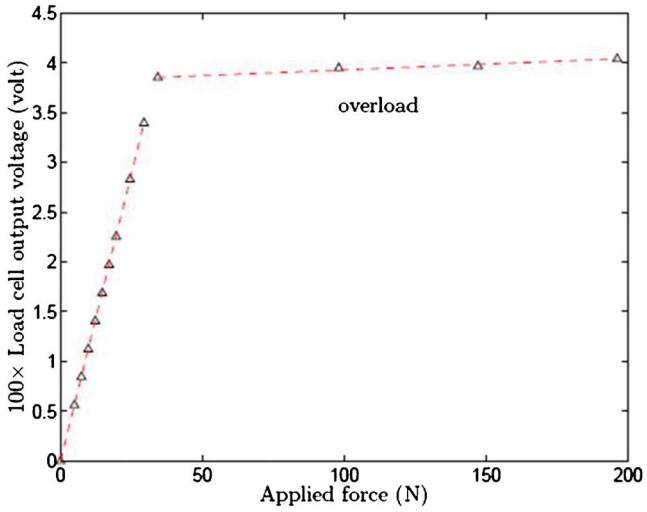

Fig. 7. Sensor output versus applied loads.

5 CONCLUSION

The design and mechanical analysis of load cell with hub-sprocket shape with donut shim for overload protection has been presented. Stress-stain analysis of such a load cell was performed to find the optimal geometry of the sensor for given values of rating load and overload ratio that maximizes the sensor sensitivity. A load cell prototype for rating force 30 N has been fabricated and tested. The voltage outputs of the sensor in response to the forces less than the rating load showed an accuracy of 0.2% of full scale. Further experimental results showed that the sensor output voltage saturated as the applied force exceeded the rating load. This clearly demonstrated the sensor's flexures were protected against overloading.

REFERENCES

1. Chang, F.-K., *Structural health monitoring, 2005: advancements and challenges for Implementation*. Pennsylvanis, U.S.A.: A DEStech Publications, IMc., 2005.
2. Mrad, M., "Potential of bragg grating sensors for aircraft health monitoring," *Transactions of the Canadian Society for Mechanical Engineering*, Vol. 31, pp. 1–17, 2007.
3. Ciniviz, M., "Performance and energy balance of a low heat rejection diesel engine operated with diesel fuel and ethanol blend," *Transactions of the Canadian Society for Mechanical Engineering*, Vol. 34, pp. 93–104, 2010.
4. Rentschler, M.E., Farritor, S.M. and Iagnemma, K.D., "Mechanical design of robotic in vivo wheeled mobility," *ASME Journal of Mechanical Design*, Vol. 129, pp. 1037–1045, 2007.
5. Saouma, V.E., Anderson, D.Z., Ostrander, K., Lee, B. and Slowik, V., "Application of fiber bragg grating in local and remote infrastructure health monitoring," *Materials and Structures*, Vol. 31, No. 2, pp. 259–266, 1998.
6. Wright, W.J., Schwartz, R.B. and Nixa, W.D., "Localized heating during serrated plastic flow in bulk metallic glasses," *Materials Science and Engineering*, Vol. 319–321, pp. 229–232, December 2001.
7. Sutherland, H., Beattie, A., Hansche, B., Musial, W., Allread, J., Johnson, J. and Summers, M., "The application of non-destructive techniques to the testing of a wind turbine blade," Sandla National Laboratories, Llvermore, California, Tech. Rep., 1994.

8. Whitten, L., Schulz, J.M., Seim, E.U. and Morrell, M., "Traffic monitoring/control and road condition monitoring using fiber optic-based systems," in *Proc. SPIE/Smart Sensors*, Vol. 3671, May 1999.
9. Otsuka, H., Takeshita, E., Yabuki, W., Wang, Y., Yoshimura, T. and Tsunomot, M., "Study on the seismic performance of reinforced concrete columns subjected to torsional moment, bending moment and axial force," in *13th World Conference on Earthquake Engineering*, Vancouver, B.C., Canada, Paper No. 393, Aug. 2004.
10. Muller, I., de Brito, R.M., Pereira, C.E. and Brusamarello, V., "Load cells in force sensing analysis - thoery and a novel application," *IEEE Instrument & Measurement Magazine*, Feb. 2010.
11. Taylor, R.P., Streele, W.G. and Douglas, F., "Uncertainty analysis of rocket motor thrust measurements with correlated biases," *ISA Transactions*, Vol. 34, No. 3, pp. 253–259, 1995.
12. de Lucena, S.E., de Aquino, M.G.S. and Caporalli-Filho, A., "A load cell for grain-propelled ballistic rocket thrust measurement," in *IEEE Instrumentation and Measurement Technology Conference*, Ottawa, Canada, pp. 1767–1772, May 2005.
13. Makabe, M. and Harada, S., "Research of protection equipment for load cell receiving a large impact load," in *SICE-ICASE International Joint Conference*, Bexco, Busan, Korea, pp. 2521–2526, Oct. 2006.
14. *The Pressure Strain and Force Handbook*, Omega Engineering, Inc., Stamford, CT, 1995.
15. *Precision Load Cells*, S. Himmelstien and Company, IL 60195, USA, 1991.
16. *Load and Torque Cells*, Interface Force Measurement Ltd., Crowthorne, Berks., UK, 1995.
17. *Load Cell and Torque Sensor Handbook*, Lebow Product Inc., Don Mills, ON, 2003.
18. Timoshenko, S., *Strength of Matrials: Part II Advanced Theory and Problems*. NY: D. Van Nostrand Co, 1941.

APPENDIX

The thermal stress induces axial force which, in turn, may cause structural instability of the beams due to buckling. According to the extended Euler's formula, the critical buckling load of a beam with two of its ends clamped is [18]

$$F_{\mathrm{cr}} = \frac{4\pi^2 EI}{L^2} \tag{23}$$

On the other hand, the axial force, F_{axial}, corresponding to temperature variation ΔT is

$$F_{\mathrm{axial}} = EA\alpha\Delta T \tag{24}$$

where $A = Wt$ is the beam's cross-section area, and α is the coefficient of thermal expansion of the sensor's material. Buckling can be avoided if $F_{\mathrm{axial}} < F_{\mathrm{cr}}$, which leads to

$$\frac{t}{L} > \frac{\sqrt{3\alpha\Delta T}}{\pi}. \tag{25}$$

For stainless steel material $\alpha = 17.3 \times 10^{-6}$ and maximum temperature variation $\Delta T = 75^{\circ}\mathrm{C}$, the right-hand side of (25) is equal to 0.02.